Materials Research Bulletin **45**, 1527-1532 (2010).

Synthesis, thermal stability, and oxygen intake/release characteristics of $YBa(Co_{1-x}Al_x)_4O_{7+\delta}$

Takafumi Komiyama, Teruki Motohashi*, Yuji Masubuchi, and Shinich Kikkawa
Graduate School of Engineering, Hokkaido University, Sapporo 060-8628, Japan
(Dated: 18 January 2010. Revised Form Dated: 26 May 2010)

The $YBaCo_4O_{7+\delta}$ (Y-114) phase has recently attracted interests as a potential oxygen storage material due to its oxygen intake/release capability at 200 ~ 400°C. Nevertheless, thermal instability of Y-114 has been an obstacle for future applications, since this compound immediately starts to decompose when the sample is heated at 700 ~ 800°C in oxygen-rich atmosphere. Here we demonstrate that Al-for-Co substitution in Y-114 drastically enhances the thermal stability. Substituting only 10 at% of aluminum for cobalt in Y-114 essentially suppresses the decomposition reaction seen at 700 ~ 800°C, while well retaining its remarkable oxygen intake/release capability at 200 ~ 400°C. It is also revealed that the addition of aluminum effectively reduces the particle size. The Al-substituted Y-114 products exhibit superior oxygen intake/release response to the Al-free products upon switching the atmosphere between O_2 and N_2.

Keywords: oxides; chemical synthesis; thermogravimetric analysis (TGA); diffusion; phase transactions

*Corresponding author
Teruki Motohashi
Graduate School of Engineering, Hokkaido University
N 13, W 8, Kita-ku, Sapporo 060-8628, JAPAN
E-mail address: t-mot@eng.hokudai.ac.jp
Tel: +81(0)11 706 6741 Fax: +81(0)11 706 6740

1. Introduction

The remarkable oxygen intake/release capability has been discovered and highlighted for a complex cobalt oxide, $YBaCo_4O_{7+\delta}$ (which is called "Y-114") [1,2]. The compound was originally reported by Valldor and Andersson in an oxygen-stoichiometric form ($\delta = 0$) [3]. The crystal structure consists of a three-dimensional network of corner-sharing CoO_4 tetrahedra, forming alternate stacking of triangular and Kagomé lattices of cobalt atoms, as illustrated in Fig. 1. The corner-sharing framework is favorable to allow modifications in the local atomic arrangement, leading to variable oxygen content. In fact, it appeared that the Y-114 phase intakes excess oxygen of $\delta \geq 1.0$ and releases it in flowing O_2 gas as the temperature increases in a narrow range of 200 ~ 400°C [1]. When excess oxygen atoms are incorporated in the crystal lattice, the formal cobalt valence accordingly increases from +2.25 ($\delta = 0$) to *e.g.* +2.75 ($\delta = 1.0$). In an oxygen-excess $YBaCo_4O_8$ phase, a part of the CoO_4 tetrahedra transforms into CoO_6 octahedra with drastic displacements of some of the oxygen sites to allow incorporating two extra O atoms [4]. Because trivalent cobalt is energetically favorable in octahedral coordination, the oxidation of divalent cobalt accompanies the tetrahedral-to-octahedral transformation. The oxygen intake/release processes are highly reversible, being controlled by both temperature and/or oxygen partial pressure.

The remarkable oxygen intake/release capability of Y-114 has made this compound a promising candidate for a new oxygen-storage material [1,2,5]. The highest oxygen content, $\delta \approx 1.5$, was achieved by means of high-pressure oxygen annealing [6]. This

value corresponds to the oxygen-storage capacity (= OSC; the amount of "mobile oxygen" stored in the crystal lattice) of 1,310 μmol-O_2/g or 4.2 wt%, being much larger than the theoretically expected value for a conventional oxygen-storage material, CeO_2-ZrO_2 (so-called "CZ"; OSC = 870 μmol-O_2/g or 2.8 wt%) [7]. Materials with such large OSCs may be advantageous for various applications, *e.g.* three-way automotive catalyst, "oxygen scavengers" for inert-gas purifications, oxidizing agent in anaerobic processes, *etc*.

In terms of practical uses, however, a critical issue of Y-114 is its thermal instability at elevated temperatures: the Y-114 phase immediately starts to decompose into a mixture of $BaCoO_{3-\delta}$ and CoO (plus debris containing Y and Co) when the sample is heated at T = 700 ~ 800°C in oxygen-rich atmospheres [1,8]. The Y-114 phase is generally synthesized at T > 900°C, followed by rapid cooling to room temperature. While the compound appears thermodynamically unstable at lower temperatures, the decomposition reaction is substantially frozen below ≈600°C, and the Y-114 phase is assumed to remain kinetically stabilized as a meta-stable phase. Hence Y-114 exhibits its unique oxygen intake/release behavior in the meta-stable state. It is highly desirable to enhance thermal stability of this material, in order to open up the possibility of high-temperature applications.

For tailoring the phase stability of Y-114, the control of chemical composition is one of the most promising routes. The Y-114 phase is indeed known to accept various kinds of cation substitutions, *e.g.* Ca and smaller rare earth elements (Dy, Ho, Er, Tm, Yb, and Lu) for Y [9-15], and Fe, Zn, Al, and Ga for Co [8,9,16-20]. Among these

substitutions, aluminum was suggested to be highly effective to suppress the thermal instability [16,21]. It was found that the decomposition temperature (T_d) is boosted up to ~700°C for a sample with the nominal composition of $YBa(Co_{0.9}Al_{0.1})_4O_{7+\delta}$ [21]. In the previous studies, however, the samples were prepared by a conventional solid-state reaction technique from powder mixture of Y_2O_3, $BaCO_3$, Co_3O_4, and Al_2O_3, such that compositional inhomogeneity might be concerned due to poor reactivity of Al_2O_3. Moreover, effects of Al-for-Co substitution on the grain morphology and microstructure of Y-114 has not been elucidated. Keeping in mind that oxygen intake/release processes involve oxygen diffusion in crystallites and redox reactions at the grain surface, the control of grain size should be of particular importance.

In the present study, a series of $YBa(Co_{1-x}Al_x)_4O_{7+\delta}$ samples was prepared by a wet-chemical synthesis technique. Thus obtained $YBa(Co_{1-x}Al_x)_4O_{7+\delta}$ samples were characterized to investigate their crystal structure, phase stability, grain morphology, and oxygen intake/release characteristics at low temperatures.

2. Experimental

Polycrystalline samples of $YBa(Co_{1-x}Al_x)_4O_{7+\delta}$ were synthesized from precursor powders prepared by an EDTA (ethylenediaminetetraacetic acid) polymerized complex method [1]. Y_2O_3 (99.9%, Wako Pure Chemicals), $Ba(NO_3)_2$ (>99%, Kanto Chemical), $Co(NO_3)_2 \cdot 6H_2O$ (>98%, Kanto Chemical), and Al metal powder (99.9%, Nilaco) were used as starting materials. Stoichiometric amounts of these powders were dissolved in a

concentrated HNO_3 solution in which EDTA/NH_3 solution was subsequently added as a complexing agent. The molar ratio between EDTA and metal ions was fixed at 1.5 : 1. The EDTA complex solution was dried and combusted in a porcelain bowl, resulting in a porous solid residue. This solid was ground, pelletized, and then fired at 1050°C in air for 20 hours, followed by rapid cooling to room temperature. The as-synthesized products were post-annealed at 500°C in flowing N_2 gas for 15 hours, in order to minimize excess oxygen in the $YBa(Co_{1-x}Al_x)_4O_{7+\delta}$ phase.

Phase purity and lattice parameters were checked for the resultant products by means of X-ray powder diffraction (XRD; Rigaku Ultima IV; Cu Kα radiation). Crystal structure was refined for the x = 0 (Al-free) and 0.10 products using the Rietveld method with RIETAN2000 software [22]. The data were collected over the angular range of 10 – 120° with a step size of 0.02° and counting times of 8.0 – 10.0 s per step. The grain morphology and microstructure were observed with a scanning electron microscope (SEM; JEOL JSM-6300F).

The thermal behaviors were investigated by means of thermogravimetry (TG; ULVAC MTS9000 and Rigaku TG8120). The measurements were carried out for specimens of ~ 30 mg in flowing O_2 up to 1000°C. The heating rate was kept slow (1°C/min) to anticipate that the thermal decomposition occurred closely in thermodynamic equilibrium. Moreover, isothermal TG experiments were performed at 300, 320, and 350°C upon switching the atmosphere from N_2 to O_2 and *vice versa* to investigate the response and reversibility of the oxygen intake/release processes.

3. Results and discussion

3.1. Structural features of $YBa(Co_{1-x}Al_x)_4O_{7+\delta}$

The $YBa(Co_{1-x}Al_x)_4O_{7+\delta}$ samples with x = 0 (Al-free), 0.05, 0.10, 0.125, 0.15, and 0.20 were synthesized and subsequently post-annealed in flowing N_2. The XRD patterns for the N_2-annealed products are displayed in Fig. 2. While the products are essentially single-phase of the Y-114 type structure up to x = 0.125, small peaks due to impurity phases (Y_2O_3, $BaAl_2O_4$, and CoO) are prominent in samples with $x \geq 0.15$. The lattice parameters for all the N_2-annealed products were determined utilizing a model-independent profile fit assuming a hexagonal unit cell and plotted in Fig. 3 as a function of the nominal Al content (x). The values for the Al-free product are close to those reported previously [1,6,8]. Both the *a*- and *c*-axis lengths linearly decrease with increasing x, and then tend to level off at $x \geq 0.15$. From these results, it is concluded that $YBa(Co_{1-x}Al_x)_4O_{7+\delta}$ forms a solid solution up to the solubility limit $x_L \approx 0.125$. The x_L value in the present work agrees well with that in Ref. 21, whereas it is somewhat smaller than $x_L \geq 0.25$ reported for a single crystalline sample by Valldor *et al*. [17]. The discrepancy is probably due to different synthesis conditions: the $YBa(Co_{0.75}Al_{0.25})_4O_{7+\delta}$ crystal in Ref. 17 was grown from a congruent melt utilizing a floating-zone mirror image furnace.

The XRD data of the Al-free (x = 0) phase were successfully refined based on the structural model that is given in the previous literatures [3,9,24]. The important

crystallographic parameters are summarized in Tables 1 and 2. The structural features of our Al-free product are in good agreement with those in the previous literature [3]. The average Co-O distance is calculated to be 0.185 nm. This is slightly larger than the value expected for the Al-O distance (0.179 nm) [23], consistent with the lattice shrinkage upon Al-for-Co substitution. Bond-valence sum (BVS) calculations show that the oxidation states at the two Co sites are comparable to each other, *i.e.* V_{Co} = +2.31 and +2.28 for the Co(1) (triangular) and Co(2) (Kagomé) sites, respectively. This suggests that, although the Co atoms are likely to have mixed valence states ($3Co^{2+}$ and $1Co^{3+}$), Co^{3+} is randomly distributed in the both sites. It should also be noted that the Ba-O distances are much larger than those expected from the ionic radii. In other words, Ba^{2+} is severely "underbonded" with an extremely low V_{Ba} value (= +1.23). We speculate that the atomic displacement may become significant at the Ba site, since each Ba atom resides in a large cavity as compared to its ionic size. This speculation is supported by the experimental fact that the displacement parameter *B* is unusually large at the Ba site (see Table 2).

For the Al-substituted (x = 0.1) phase, on the other hand, refinements were performed assuming the isostructure of the Al-free phase. To ascertain whether substituted Al atoms preferably occupy a specific Co site, the following three models were examined: *Model 1*: all the Al atoms occupy the Co(1) site. *Model 2*: all the Al atoms occupy the Co(2) site. *Model 3*: the Al atoms are distributed in the both Co sites. The refinement with *Model 3* gave the smallest R_{wp} value (9.18%) with a reasonable figure-of-merit (S = 1.75). Meanwhile, the refinements with *Models 1 and 2* resulted in relatively larger R_{wp} values (= 9.78 and 9.37%, respectively). Hence, *Model 3* is the best

to describe the structure of the Al-substituted phase. Crystallographic parameters of the Al-substituted phase are also summarized in Tables 1 and 2. Our Rietveld analysis suggests that Co/Al mixing occurs at the both two sites, involving a tendency of Al enrichment at the Co/Al(1) site. This feature is consistent with the fact that both of the Co/Al-O_4 tetrahedra are shrunk upon Al-for-Co substitution, while the average Co/Al-O distance is slightly shorter at Co/Al(1) than at Co/Al(2).

3.2. Grain microstructure of the $YBa(Co_{1-x}Al_x)_4O_{7+\delta}$ products

Figure 4 shows typical SEM images of the single-phase products with x = 0, 0.05, 0.10, and 0.125. It is seen that all the products consist of porous agglomerates of fine primary particles. The SEM images demonstrate that these products are uniform in terms of particle size and morphology, suggestive of high degree of chemical homogeneity owing to the wet-chemical synthesis route. The average size of the primary particles is decreased with increasing Al content (x), from ~2.5 μm for the Al-free (x = 0) product to ~1.0 μm for the x = 0.10 and 0.125 products. Thus, it is obvious that the addition of aluminum contributes to the reduction of the particle size. We interpret this effect to mean that the added Al contributes effectively suppresses the grain growth of Y-114. This finding is remarkable from a practical point of view, since the reduced particle size would have positive impacts on the oxygen intake/release characteristics.

3.3. Thermal stability of the $YBa(Co_{1-x}Al_x)_4O_{7+\delta}$ phase at high temperatures

Shown in Fig. 5 are TG curves recorded for the x = 0, 0.05, 0.10, and 0.125 products in flowing O_2 gas between 100 and 1000°C. The Al-free (x = 0) product exhibits two prominent humps. The first hump at 200 ~ 400°C is related to the unique oxygen intake/release phenomena of the Y-114 phase [1]. The second one at high temperatures corresponds to the phase decomposition [1,8]. The decomposition involves a large weight gain due to oxygen intake which leads to the formation of more highly oxidized $BaCoO_{3-\delta}$. This oxygen-intake behavior is not preferable in terms of the oxygen storage capability, since the decomposition and the subsequent recovery of the phase are accompanied by changes in the grain microstructure.

These thermal behaviors are found to be greatly influenced by the Al-for-Co substitution. The first hump is suppressed in the x = 0.125 product, while the height of the hump remains almost unchanged for x = 0, 0.05 and 0.10. This indicates that Al-substituted Y-114 retains its oxygen storage capability up to x = 0.10. In terms of the second hump, the onset temperature is increased from ≈650°C to ≈750°C in the x = 0.05 product. Furthermore, the second hump almost disappears for x = 0.10.

To ensure the modification in thermal behaviors in the Al-substituted phase, the following experiment was carried out. Small portions of the Al-free (x = 0) and Al-substituted (x = 0.10) products were kept at 500, 600, 700, 800, and 900°C for 20 hours in air, and subsequently quenched to room temperature within 1 minute. The XRD analysis on the quenched samples reveals that the Al-free samples completely

decompose into $BaCoO_{3-\delta}$ and CoO (plus debris containing Y and Co) at 700 and 800°C [Fig. 6(a)]. As reported previously [1,8], the Al-free phase is thermally unstable in this temperature range, while this phase is considered to be thermodynamically stable above 900°C and kinetically meta-stable below 600°C. In contrast, the XRD patterns for the Al-substituted samples remain unchanged in the whole temperature range studied [Fig. 6(b)]. Sharp and intense diffraction peaks indicate that the Al-substituted phase retains its good crystallinity even after the heat treatment at 500 ~ 900°C.

It is thus concluded that substituting only 10 at% of aluminum at the cobalt sites essentially suppresses the decomposition reaction of Y-114. The Al-substitution effect can be discussed from a structural point of view. The decomposition of Y-114 may be related to the tendency of cobalt to adopt octahedral coordination, since cobalt is in octahedral coordination in the decomposition products (such as $BaCoO_{3-\delta}$ and CoO) [20]. Suppose the Y-114 phase is kinetically stabilized at low temperatures, it tends to accept excess oxygen atoms to form octahedral coordination of trivalent cobalt, instead of the phase decomposition. The improved thermal stability of the Al-substituted phase is mainly attributed to a more stabilized lattice framework. It is likely that a stronger tetrahedral-site preference of aluminum than cobalt effectively suppresses the decomposition reaction. In fact, improved thermal stability was also reported for Zn-for-Co substituted Y-114, in which substituted zinc atoms are believed to increase the tetrahedral-site preference of cations [20].

In the previous work [21], small amounts of decomposition products were detected for $x = 0.10$ when quenched from 700 and 750°C. This is in contrast to the present result

in which our x = 0.10 product, prepared by the wet-chemical synthesis route, retains its phase stability in the whole temperature range studied. We interpret that the partial decomposition of the x = 0.10 product in the previous work is due to inferior chemical homogeneity. Since the sample in Ref. 21 was prepared through the conventional solid-state reaction, local fluctuation of the chemical composition would be inevitable. It is reasonable to assume that some grains decomposed at 700 and 750°C due to their insufficient Al concentration to overcome the phase instability.

3.4. Oxygen intake/release characteristics of $YBa(Co_{1-x}Al_x)_4O_{7+\delta}$

To investigate the response and reversibility of the oxygen intake/release processes in $YBa(Co_{1-x}Al_x)_4O_{7+\delta}$, isothermal TG curves were measured at 300, 320, and 350°C upon switching the atmosphere between O_2 and N_2 (Fig. 7). At 350°C, both of the Al-free (x = 0) and Al-substituted (x = 0.10) products show oxygen intake/release behaviors in a highly reversible manner. For the Al-substituted product, the maximum amount of incorporated oxygen is 1.1 wt%, being much smaller than ≈2.9 wt% for the Al-free product. The smaller oxygen amount is also found at 320°C. These results are consistent with the TG data presented in Fig. 5, where the sample weight of the x = 0.10 product is maximal at 300°C, and then decreasing at elevated temperatures.

One may notice that the weight gain/loss at 350°C tends to level off within a shorter period in the Al-substituted product than the Al-free one, indicating that the kinetics of oxygen intake/release is accelerated by Al substitution. This feature is more

pronounced in TG data recorded at 300 and 320°C: that is, the Al-substituted Y-114 products exhibit superior characteristics in terms of the oxygen intake/release response at lower temperatures. We attribute the improved response of oxygen intake/release to the modification in the grain microstructure upon Al substitution. The reduced particle size in the Al-substituted products, as clearly demonstrated in Fig. 4, is most likely to contribute to the faster oxygen intake/release rates. Needless to say, better response is one of the most important aspects for practical uses.

At 300°C, the maximum weight gain exceeds 3.8 wt% for the Al-substituted product, even larger than the value obtained for the Al-free product. However, the weight gain severely decreases in the repeated oxygen intake/release processes from 3.8, 3.4 to 2.9 wt% in the 1st, 2nd, and 3rd cycles, respectively. With a careful look at the TG curve, the oxygen intake rate in the 2nd/3rd cycles appears to be much slower than in the 1st cycle. Apparently, the decrease in the oxygen intake rate leads to poor cycling characteristics of the Al-substituted product at this temperature.

This feature is presumably attributed to a structural reconstruction involved by aluminum. We assume that upon oxygen intake a part of the substituted Al atoms has bound to excess oxygen to form AlO_6 octahedra. Such AlO_6 octahedra, which are locally stabilized due to stronger affinity between Al and O ions, would act as effective barriers for oxygen diffusion. In the repeated cycles the number of the AlO_6 octahedra increases, leading to the further decrease in the oxygen intake rate. A slow rate of oxygen intake was also reported for $YBa(Co_{0.99}Fe_{0.01})_4O_{7+\delta}$, suggesting that a similar structure reconstruction takes place also in the Fe-substituted Y-114 [19].

4. Conclusion

Polycrystalline samples of $YBa(Co_{1-x}Al_x)_4O_{7+\delta}$ were synthesized and characterized to investigate effects of Al-for-Co substitution on the phase stability, grain morphology, and oxygen intake/release characteristics of the pristine $YBaCo_4O_{7+\delta}$ (= Y-114) phase. We demonstrate that substituting only 10 at% of aluminum for cobalt in Y-114 essentially suppresses the decomposition reaction seen at 700 ~ 800°C, while well retaining its remarkable oxygen intake/release capability at 200 ~ 400°C. It is also revealed that the addition of aluminum effectively reduces the particle size to exhibit superior oxygen intake/release response. It is thus concluded that Al-substituted Y-114 is a potential material for various high-temperature applications based on its oxygen storage capability.

Acknowledgement

The authors thank H. Yamauchi, M. Karppinen, and S. Räsänen of Helsinki University of Technology for their fruitful discussion and comments. The present work was supported by a Grant for R & D of New Interdisciplinary Fields in Nanotechnology and Materials Program of MEXT of Japan.

References

[1] M. Karppinen, H. Yamauchi, S. Otani, T. Fujita, T. Motohashi, Y. -H. Huang, M. Valkeapää, and H. Fjellvåg, Chem. Mater. **18** (2006) 490.

[2] M. Karppinen, H. Yamauchi, H. Fjellvåg, and T. Motohashi, PCT/JP2006313436, Int. Patent Appl., filed June 6, 2006.

[3] M. Valldor and M. Andersson, Solid State Sci. **4** (2002) 923.

[4] O. Chmaissem, H. Zheng, A. Huq, P. W. Stephens, and J. F. Mitchell, J. Solid State Chem. **181** (2008) 664.

[5] T. Motohashi, S. Kadota, H. Fjellvåg, M. Karppinen, and H. Yamauchi, Mater. Sci. Eng. B **148** (2008) 196.

[6] S. Räsänen, H. Yamauchi, and M. Karppinen, Chem. Lett. **37** (2008) 638.

[7] see *e.g.*, J. Kašpar and P. Fornasiero, J. Solid State Chem. **171** (2003) 19.

[8] E.V. Tsipis, V. V. Kharton, J. R. Frade, and P. Núnez, J. Solid State Electrochem. **9** (2005) 547; E. V. Tsipis, V. V. Kharton, and J. R. Frade, Solid State Ionics **177** (2006) 1823.

[9] M. Valldor, Solid State Sci. **6** (2004) 251.

[10] G. L. Bychkov, S. N. Barilo, S. V. Shiryaev, D. V. Sheptyakov, S. N. Ustinovich, A. Podlesnyak, M. Baran, R. Szymczak, and A. Furrer, J. Cryst. Growth **275** (2005) e813.

[11] N. Nakayama, T. Mizota, Y. Ueda, A. N. Sokolov, and A. N. Vasiliev, J. Mag. Mag. Mater. **300** (2006) 98.

[12] A. Huq, J. F. Mitchell, H. Zheng, L.C. Chapon, P. G. Radaeli, K. S. Knight, and P. W. Stephens, J. Solid State Chem. **179** (2006) 1136.

[13] A. Maignan, V. Caignaert, D. Pelloquin, S. Hébert, V. Pralong, J. Hejtmanek, D. Khomskii, Phys. Rev. B **74** (2006) 165110.

[14] S. Kadota, M. Karppinen, T. Motohashi, and H. Yamauchi, Chem. Mater. **20** (2008) 6378.

[15] H. Hao, J. Cui, C. Chen, L. Pan, J. Hu, and X. Hu, Solid State Ionics **177** (2006) 631.

[16] S. Wang, H. Hao, B. Zhu, J. Jia, and X. Hu, J. Mater. Sci. **43** (2008) 5385.

[17] M. Valldor, N. Hollmann, J. Hemberger, and J. A. Mydosh, Phys. Rev. B **78** (2008) 024408.

[18] A. Maignan, V. Caignaert, V. Pralong, D. Pelloquin, and S. Hébert, J. Solid State Chem. **181** (2008) 1220.

[19] E. V. Tsipis, J. C. Waerenborgh, M. Avdeev, and V. V. Kharton, J. Solid State Chem. **182** (2009) 640.

[20] J.- H. Kim and A. Manthiram, Chem. Mater. (2009) in press.

[21] S. Räsänen, T. Motohashi, H. Yamauchi, and M. Karppinen, J. Solid State Chem. (2010) in press.

[22] F. Izumi and T. Ikeda, Mater. Sci. Forum **321-324** (2000) 198.

[23] R. D. Shannon and C. T. Prewitt, Acta Cryst. **B25** (1969) 925; R. D. Shannon, Acta Cryst. **A32** (1976) 751.

[24] A recent work by Caignaert *et al.* [Solid State Sci. **8** (2006) 1160] suggested that the crystal structure of $YBaCo_4O_7$ is better to be described with orthorhombic space group $Pbn2_1$ rather than hexagonal $P6_3mc$. Nevertheless, it is practically impossible to differentiate between these structural models by means of the conventional XRD technique, since the $Pbn2_1$ model only involves slight displacements from the special positions for the $P6_3mc$ model. High-resolution neutron diffraction data would be needed to discuss such small displacements. We thus adopted the hexagonal $P6_3mc$ model to refine the structure of our $YBa(Co_{1-x}Al_x)_4O_{7+\delta}$ products.

[25] K. Momma and F. Izumi, J. Appl. Crystallogr. **41** (2008) 653.

Table 1. Rietveld refinement details for the Al-free (x = 0) and Al-substituted (x = 0.10) phases. The interatomic distances (d) and bond-valence sums (V) were calculated utilizing VESTA program [25].

	Al-free (x = 0)	Al-substituted (x = 0.10)
crystal system	hexagonal	hexagonal
space group	$P6_3mc$	$P6_3mc$
a (nm)	0.63031(16)	0.62922(13)
c (nm)	1.02435(19)	1.02341(16)
volume (10^{-27} m^3)	0.35245(14)	0.35090(12)
Z	2	2
calc. density (10^3 kg m^{-3})	5.408	5.311
$d_{Y\text{-}O}$ (nm)	(3×) 0.2260	(3×) 0.2230
	(3×) 0.2301	(3×) 0.2322
V_Y	2.97	3.02
$d_{Ba\text{-}O}$ (nm)	(3×) 0.2970	(3×) 0.2973
	(6×) 0.3152	(6×) 0.3146
	(3×) 0.3313	(3×) 0.3304
V_{Ba}	1.23	1.24
$d_{Co1\text{-}O}$ (nm)	(3×) 0.1727	(3×) 0.1735
	(1×) 0.1974	(1×) 0.1964
V_{Co1}	2.31	2.33
$d_{Co2\text{-}O}$ (nm)	(1×) 0.1793	(1×) 0.1824
	(2×) 0.1912	(2×) 0.1892
	(1×) 0.2018	(1×) 0.2014
V_{Co2}	2.28	2.28
R_{wp}	10.92	9.18
R_e	5.92	5.25
S	1.85	1.75

Table 2. Atomic parameters for the Al-free (x = 0) and Al-substituted (x = 0.10) phases.

atom	Wyckoff site	g	x	y	z	B (10^{-2} nm^2)
Al-free (x = 0)						
Y	2*b*	1.0	2/3	1/3	0.8796(2)	0.38(8)
Ba	2*b*	1.0	2/3	1/3	0.5000(0)	1.94(9)
Co1	2*a*	1.0	0	0	0.4232(7)	0.22(8)
Co2	6*c*	1.0	0.1712(2)	0.8288(2)	0.6804(4)	0.92(4)
O1	6*c*	1.0	0.5061(7)	0.4938(7)	0.7341(9)	1.0*
O2	2*a*	1.0	0	0	0.2546(15)	1.0*
O3	6*c*	1.0	0.1634(7)	0.8366(7)	0.5056(12)	1.0*
Al-substituted (x = 0.10)						
Y	2*b*	1.0	2/3	1/3	0.8792(2)	0.00(6)
Ba	2*b*	1.0	2/3	1/3	0.5000(0)	2.01(7)
Co/Al1	2*a*	0.85(1)/0.15(1)	0	0	0.4233(6)	0.61(9)
Co/Al2	6*c*	0.92(1)/0.08(1)	0.1713(2)	0.8287(2)	0.6800(3)	0.73(4)
O1	6*c*	1.0	0.5037(6)	0.4963(6)	0.7330(7)	1.0*
O2	2*a*	1.0	0	0	0.2538(12)	1.0*
O3	6*c*	1.0	0.1644(6)	0.8356(6)	0.5020(9)	1.0*

*The displacement parameters (B) at the oxygen sites were fixed at 1.0×10^{-2} nm^2 in the refinements.

Figure captions

Fig. 1.
Schematic illustration of the crystal structure of $YBaCo_4O_{7+\delta}$ ($\delta = 0$).

Fig. 2.
X-ray powder diffraction patterns for the N_2-annealed products of $YBa(Co_{1-x}Al_x)_4O_{7+\delta}$ with $x = 0$ (Al-free), 0.05, 0.10, 0.125, 0.15, and 0.20. Diffraction peaks for the $x = 0$ product are indexed based on a hexagonal unit cell. Peaks due to Y_2O_3, CoO, and $BaAl_2O_4$ are marked with circles, triangles, and diamonds, respectively.

Fig. 3.
The hexagonal *a*- and *c*-axis lengths for the $YBa(Co_{1-x}Al_x)_4O_{7+\delta}$ products ($\delta \approx 0$) with respect to the Al content (x). The values for the Al-free phase in previous literatures are also plotted.

Fig. 4.
SEM images of the $YBa(Co_{1-x}Al_x)_4O_{7+\delta}$ products: upper left panel, $x = 0$ (Al-free); upper right, $x = 0.05$; lower left, $x = 0.10$; lower right, $x = 0.125$.

Fig. 5.
TG curves for the $YBa(Co_{1-x}Al_x)_4O_{7+\delta}$ products with $x = 0$ (Al-free), 0.05, 0.10, and 0.125 recorded in flowing O_2 between 100 and 1000°C (heating rate 1°C/min).

Fig. 6.
X-ray diffraction patterns for (a) $x = 0$ and (b) $x = 0.10$. Small portions of each product were kept at various temperatures for 20 hours in air, and subsequently quenched to room temperature within 1 minute. Diffraction peaks due to the decomposition products, CoO and $BaCoO_{3-\delta}$, are marked with circles and triangles in Fig. 6(a), respectively.

Fig. 7.
Isothermal TG curves for the $x = 0$ and $x = 0.10$ samples at 300 (bottom), 320 (middle), and 350°C (upper) in flowing N_2 and then O_2, and *vice versa*. The data for $x = 0$ and $x = 0.10$ are shown with black and red curves, respectively.

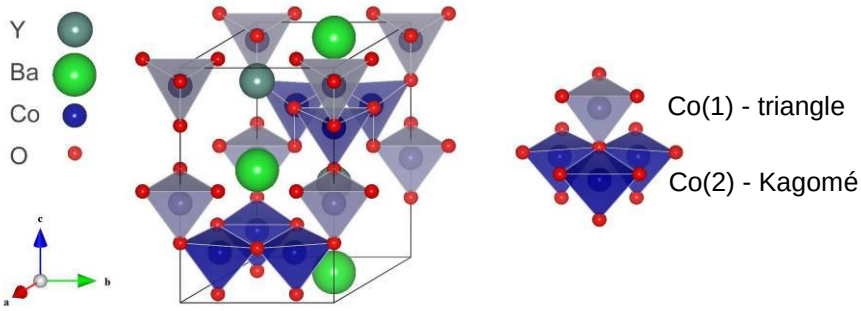

Fig. 1. Komiyama *et al.*

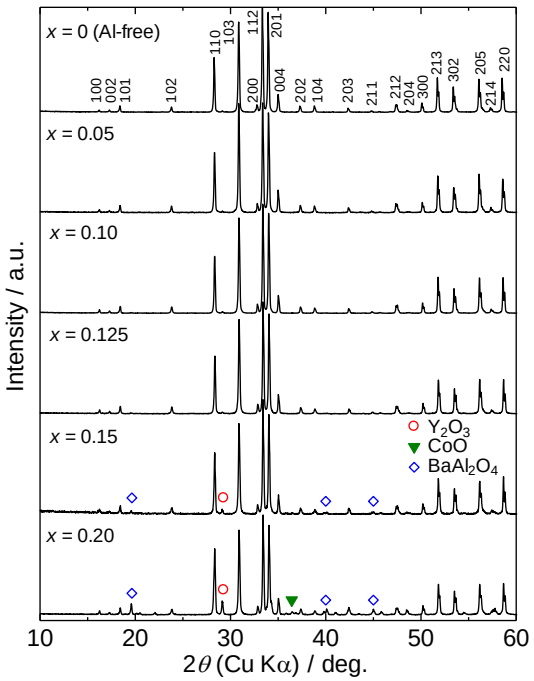

Fig. 2. Komiyama *et al.*

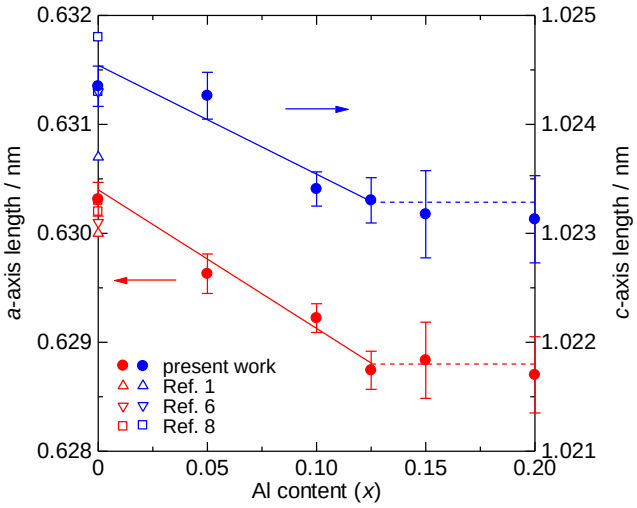

Fig. 3. Komiyama *et al.*

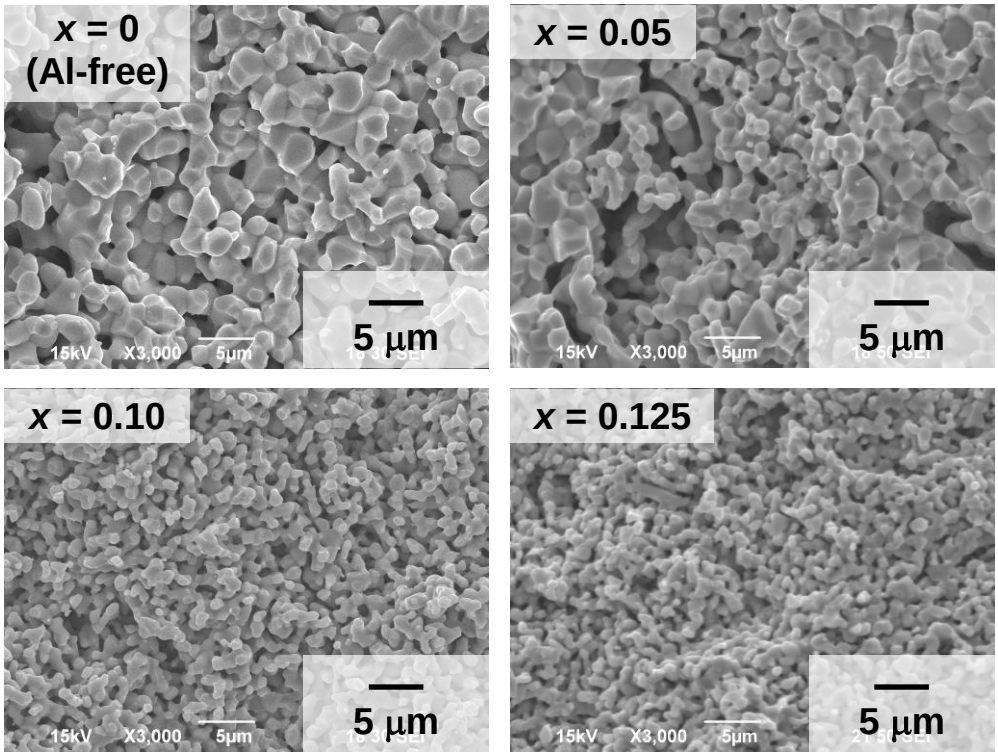

Fig. 4. Komiyama *et al*.

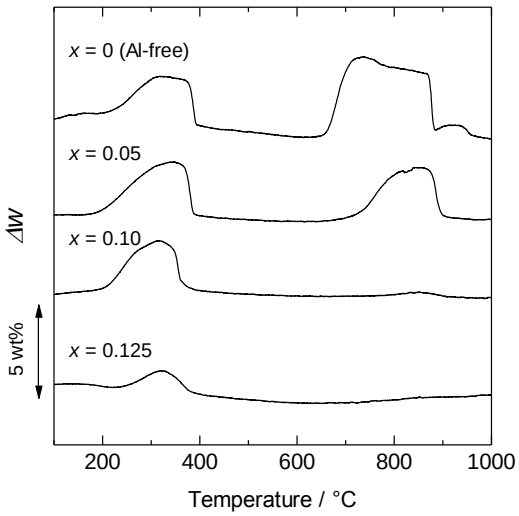

Fig. 5. Komiyama *et al.*

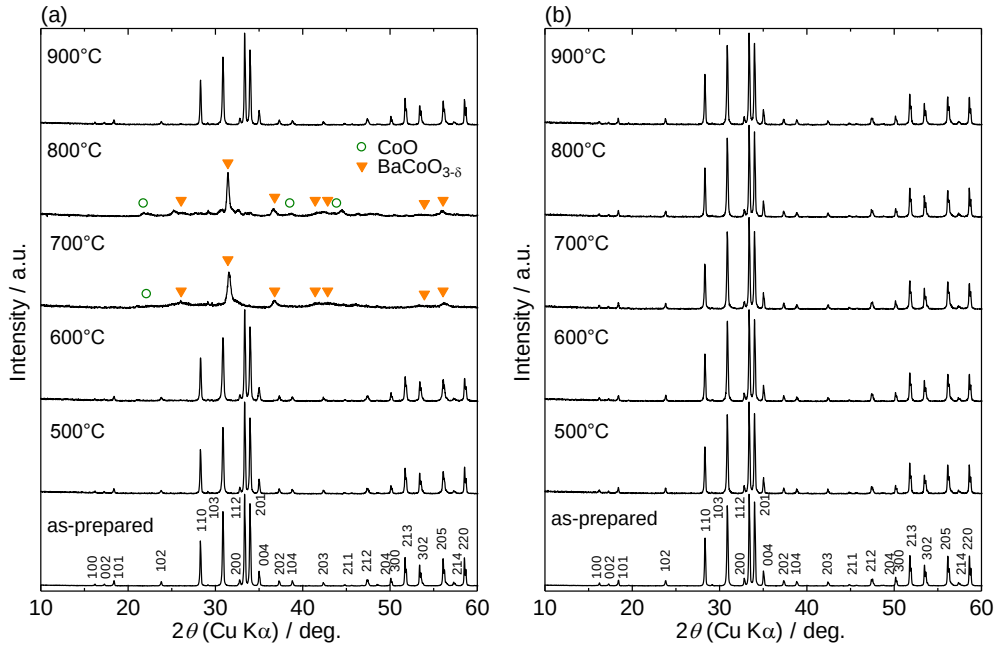

Fig. 6. Komiyama *et al.*

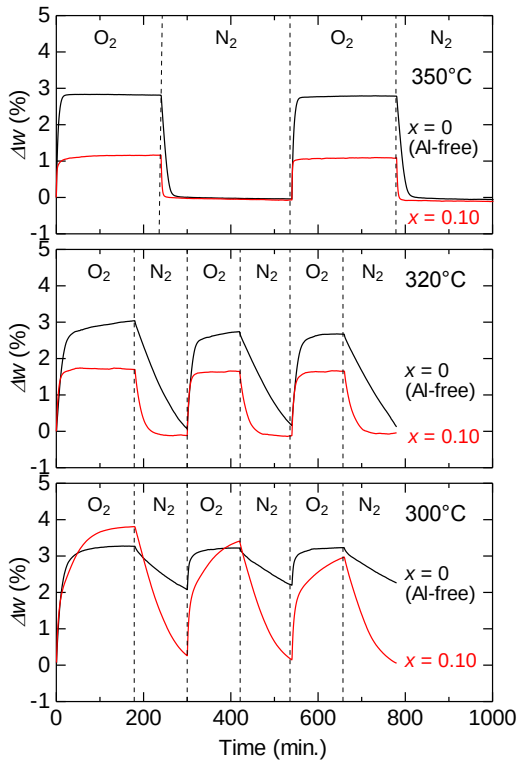

Fig. 7. Komiyama *et al.*